



HAL
open science

Evidence for hard and soft substructures in thermoelectric SnSe

Srinivasa Rao Popuri, Michaël Pollet, Rodolphe Decourt, Mihai S. Viciu,
Jan-Willem G. Bos

► **To cite this version:**

Srinivasa Rao Popuri, Michaël Pollet, Rodolphe Decourt, Mihai S. Viciu, Jan-Willem G. Bos. Evidence for hard and soft substructures in thermoelectric SnSe . Applied Physics Letters, 2017, 110 (25), 253903 (4 p.). 10.1063/1.4986512 . hal-01569393

HAL Id: hal-01569393

<https://hal.science/hal-01569393>

Submitted on 26 Jul 2017

HAL is a multi-disciplinary open access archive for the deposit and dissemination of scientific research documents, whether they are published or not. The documents may come from teaching and research institutions in France or abroad, or from public or private research centers.

L'archive ouverte pluridisciplinaire **HAL**, est destinée au dépôt et à la diffusion de documents scientifiques de niveau recherche, publiés ou non, émanant des établissements d'enseignement et de recherche français ou étrangers, des laboratoires publics ou privés.

Evidence for hard and soft substructures in thermoelectric SnSe

S. R. Popuri,^a M. Pollet,^{b,c} R. Decourt,^{b,c} M. L. Viciu^d and J. W. G. Bos^{a*}

^a *Institute of Chemical Sciences and Centre for Advanced Energy Storage and Recovery, School of Engineering and Physical Sciences, Heriot-Watt University, Edinburgh, EH14 4AS, United Kingdom.*

^b *CNRS, ICMCB, UPR 9048, Pessac F-33600, France*

^c *University of Bordeaux, UPR 9048, Pessac F-33600, France*

^d *Department of Chemistry and Applied Biosciences, ETH Zürich, Vladimir-Prelog-Weg 1, Zürich CH 8093, Switzerland*

j.w.g.bos@hw.ac.uk; michael.pollet@icmcb.cnrs.fr

SnSe is a topical thermoelectric material with a low thermal conductivity which is linked to its unique crystal structure. We use low-temperature heat capacity measurements to demonstrate the presence of two characteristic vibrational energy scales in SnSe with Debye temperatures $\theta_{D1} = 345(9)$ K and $\theta_{D2} = 154(2)$ K. These hard and soft substructures are quantitatively linked to the strong and weak Sn-Se bonds in the crystal structure. The heat capacity model successfully predicts the temperature evolution of the unit cell volume, confirming that this two-substructure model captures the basic thermal properties. Comparison with phonon calculations reveals that the soft substructure is associated with the low energy phonon modes that are responsible for the thermal transport. This suggests that searching for materials containing highly divergent bond distances should be a fruitful route for discovering low thermal conductivity materials.

Thermoelectric generation is a promising technology that enables waste heat to be converted in useful electricity.¹ There are many possible applications but widespread use has been limited by the lack of cost effective efficient thermoelectric materials. The underpinning problem is the need to optimise competing materials parameters. This is commonly expressed by the thermoelectric figure of merit, $zT = (S^2/\rho\kappa)T$, where S and ρ are the Seebeck coefficient and electrical resistivity, κ is the sum of the lattice and electronic thermal conductivities, and T is the absolute temperature. Many of

the current best thermoelectric materials are based on low lattice thermal conductivities. For example, PbTe-based nanocomposites routinely achieve $\kappa < 1 \text{ W m}^{-1} \text{ K}^{-1}$ and ZT values between 1.5 and 2 are now common.²⁻⁴ A common factor in these materials with ultralow thermal conductivities is the presence of chemically inert lone-pairs.^{5,6} Recently, outstanding thermoelectric performance (ZT = 2.5) was discovered in SnSe single crystals without any carrier doping to optimise the power factor or nanostructuring to minimize the thermal conductivity.⁷ The large ZT values are primarily based on an ultralow lattice thermal conductivity $\kappa_{\text{lat}} = 0.2\text{-}0.3 \text{ W m}^{-1} \text{ K}^{-1}$ at 800-900 K. This was attributed to the highly anharmonic bonding, leading to very strong phonon-phonon scattering, and the anisotropic crystal structure.⁷⁻¹² The crystal structure can be understood as a highly distorted rock salt derivative.^{13,14} At high-temperatures, adjacent two-atom thick rock salt layers are translated by $a/2$ so that Sn is coordinated by 5 Se atoms in the rocksalt layer and by 2 Se atoms in an adjacent layer. Upon cooling below 800 K, the structure undergoes a displacive phase transition, which leads to a strongly distorted Sn coordination polyhedron with three short and two long bonds within the rocksalt layer, and a single long bond connecting to an adjacent rocksalt layer (Fig. 1). There is recent controversy regarding the intrinsic thermal conductivity in SnSe,^{15,16} with a new single crystal study suggesting that $\kappa_{\text{lat}} \approx 2 \text{ W m}^{-1} \text{ K}^{-1}$ within the tightly bound rocksalt layers and $\sim 1 \text{ W m}^{-1} \text{ K}^{-1}$ in the perpendicular direction (300 K values).¹⁷ In polycrystalline samples a range of κ_{lat} values have been reported,¹⁸⁻²² with some suggestion that disorder is able to reduce κ_{lat} .^{21,23} The measured κ_{lat} values have also been reported to be sensitive to oxidation.²⁴ However, the promise of SnSe as an outstanding thermoelectric material is not in doubt as Na-doped single crystals show greatly improved thermoelectric power factors near room temperature and compete with the best known Bi₂Te₃ based alloys in terms of their efficiency.^{25,26}

In this Letter, we report an investigation into the low-temperature heat capacity of SnSe and combine this with crystal structure data to yield important new insights into the thermal behaviour of SnSe. Despite the fundamental importance of the heat-capacity for understanding the thermal transport, quantitative analysis of the low-temperature heat capacity has not been reported. The heat

capacity of SnSe was measured using a Quantum Design Physical Property Measurement System, and matched well with high-temperature data reported previously.²³ The SnSe sample used was highly pure with < 1 wt% SnO₂ or other impurities.²³ Neutron powder diffraction data were collected using the HRPD instrument at ISIS, Rutherford Appleton Laboratory, UK. A full structural study will be published elsewhere²⁷ and only the obtained cell volume and thermal displacement parameter are reported here.

The temperature dependence of the thermal displacement parameters gives a first insight into the vibrational properties of Sn and Se. The temperature dependence of U_{iso} for Sn and Se are shown in Fig. 1b. The U_{iso} values are large, in particular for Sn²⁺, which is typical for lone-pair containing rocksalt-based thermoelectrics.²⁸ The U_{iso} 's tend toward zero at low temperatures, demonstrating that the structure does not contain significant static disorder.

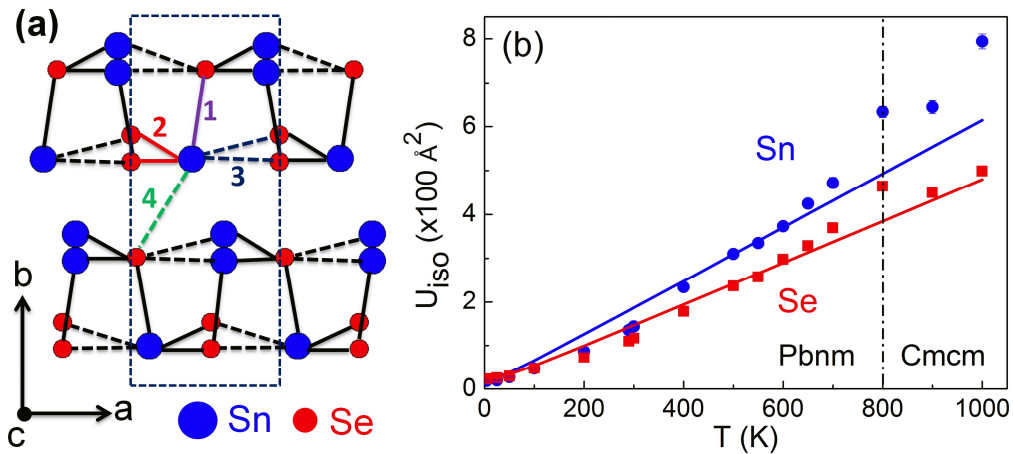


Fig. 1. (a) schematic of the low-temperature SnSe crystal structure (Pbnm setting). Important bond distances are indicated. The 300 K values for the bond distances are as follows: $d_1 = 2.75 \text{ \AA}$; $d_2 = 2.79 \text{ \AA}$; $d_3 = 3.34 \text{ \AA}$ and $d_4 = 3.47 \text{ \AA}$. (b) Temperature dependence of the isotropic thermal displacement parameters. The solid lines are fits described in the text.

In order to obtain an estimate of the characteristic energy scales of the atomic motions the U_{iso} 's for Sn and Se were fitted using:²⁹

$$U_{iso} = \frac{3\hbar^2}{mk_B\theta_D} \left[\frac{1}{4} + \left(\frac{T}{\theta_D} \right)^2 \int_0^{\theta_D/T} \frac{x}{e^x - 1} dx \right] + \sigma^2 \quad (1)$$

Here, \hbar is the reduced Planck constant, k_B is Boltzmann's constant, θ_D is the Debye temperature and σ^2 is the displacement correlation function. In both cases $\sigma^2 = 0$, confirming the absence of significant static structural disorder. The fitted θ_D values are 140(2) K for Sn and 195(3) K for Se, and the fits are shown in Fig. 1. The 40% larger value for Se is in line with expected trends based on the atomic mass and bond strength. Interestingly, the model starts to deviate from the data above 600 K, which corresponds to the onset of the structural phase transition.¹³

The temperature dependence of the heat capacity (C_p) is given in Fig. 2a, and is characterised by a linear increase beyond the Dulong-Petit value of $3R/\text{atom}$, consistent with the high-temperature data in the literature.^{7, 9, 19, 23} A plot of C_p/T versus T^2 reveals that there is no electronic contribution to the heat capacity at low-temperature, which is in keeping with the semiconducting nature of SnSe (Fig. 2b). A plot of C_p/T^3 versus T reveals an additional low-temperature contribution, which could arise from the contribution of either an Einstein mode or a Schottky anomaly to the specific heat (Fig. 2c).

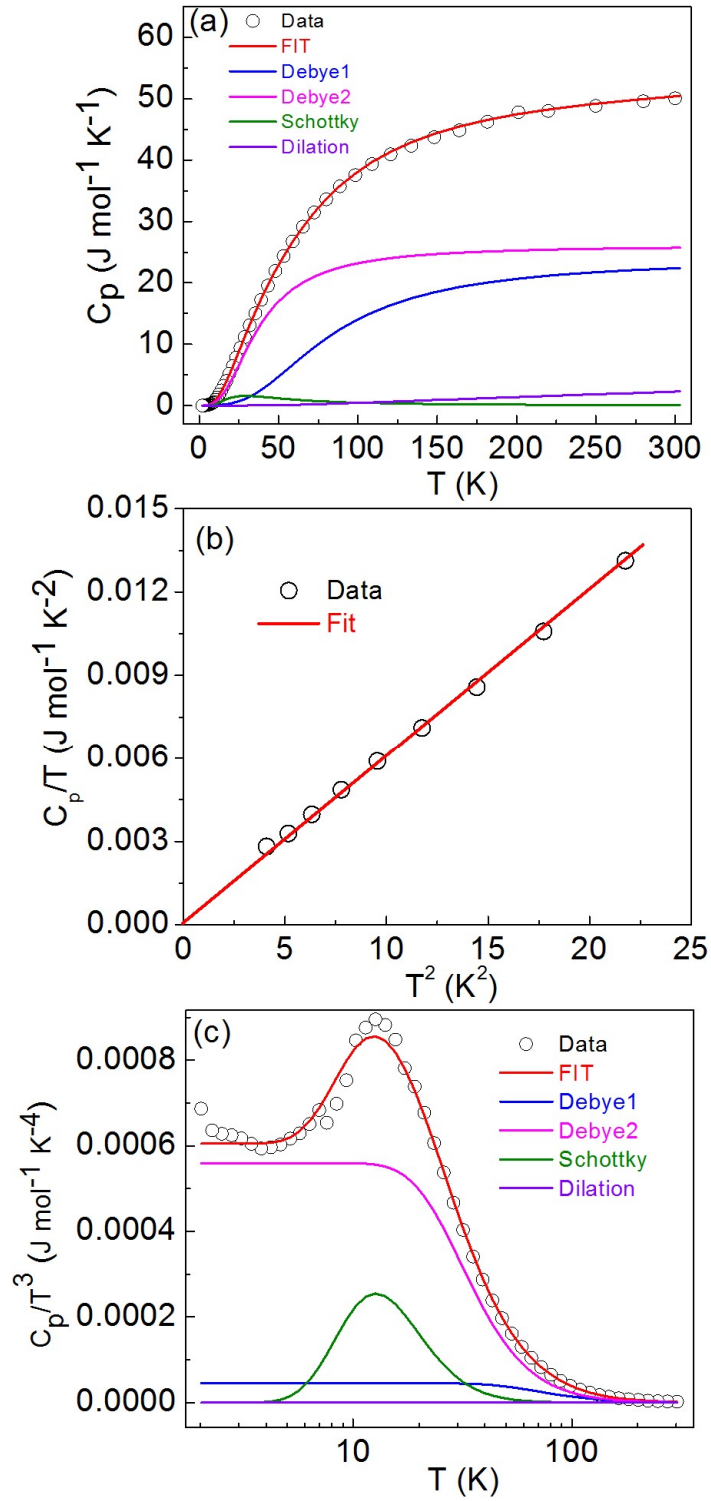


Fig. 2: (a) Fit to the temperature dependence of the heat capacity (C_p) of SnSe using two Debye terms (blue and pink line), Schottky mode (green line) and lattice dilation (purple line). The fitting procedure is described in the text. (b) C_p/T versus T^2 illustrating the absence of a significant electronic contribution to C_p . (c) C_p/T^3 versus T , highlighting the Schottky contribution at low temperatures.

Several models using combinations of Debye and Einstein (or Schottky) modes were tried. The most satisfactory fit was obtained using two Debye terms for the acoustic phonon bath, a low-temperature Schottky contribution to model the peak visible on the C_p/T^3 versus T curve and a lattice dilation term³⁰ to account for the linear increase at high temperature:

$$C_p = \sum_{i=1}^2 \left[9n_i R \left(\frac{T}{\theta_{D_i}} \right)^3 \int_0^{\theta_{D_i}/T} \frac{x^4 e^x}{(e^x - 1)^2} dx \right] + R \frac{g \left(\frac{\Delta}{T} \right)^2 e^{-\Delta/T}}{(1 + g e^{-\Delta/T})^2} + 9Bv\alpha^2 T \quad (2)$$

Here, n_i is the number of oscillators for each Debye term, R is the gas constant, θ_{D_i} are Debye temperatures, Δ is the energy gap for a two-level Schottky system and g is the ratio of the degeneracies of the lower level to the upper level, $B = 31$ GPa is the isothermal bulk modulus,³¹ v is the volume per atom and α is the thermal expansion coefficient. The thermal expansion coefficient was derived from the temperature evolution of the cell volume as $\alpha = (1/V)(dV/dT)_p$. The cell volume was fitted simultaneously (Fig. 3) using the following expression, which was adapted from Hayward et al.³² to include two Debye terms:

$$V = V_0 + a \sum_{i=1}^2 \left[\int_0^T 9n_i R \left(\frac{T}{\theta_{D_i}} \right)^3 \int_0^{\theta_{D_i}/T} \frac{x^4 e^x}{(e^x - 1)^2} dx \right] \quad (3)$$

The fitted values are $n_1 = 0.96(4)$, $n_2 = 1.04(4)$, $\theta_{D1} = 345(9)$ K, $\theta_{D2} = 154(2)$ K, $g = 0.38(2)$, $\Delta = 64(1)$ K and $V_0 = 210.32 \text{ \AA}^3$, $a = 1.8 \times 10^{-4}$. The model for C_p takes into account all important features of the data including the low temperature peak and the linear increase at higher temperature (Fig. 2). The $V(T)$ data are fitted well below 600 K, while the experimental volume expands more rapidly at elevated temperatures (Fig. 3). The thermal expansion $\alpha(T)$ has a broad maximum near 550-600 K (inset to Fig. 3), which is in good agreement with the onset of the structural phase transition.¹³

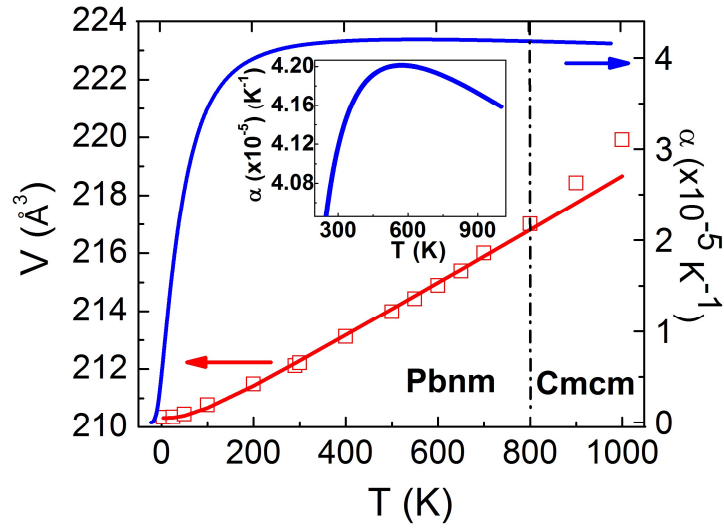


Fig. 3. Temperature dependence of the unit cell volume (red circles) and volume thermal expansion coefficient (blue line) of SnSe. The latter was derived from the fit to the volume data as described in the text.

The C_p fit reveals the presence of two Debye oscillators with different energy scales but almost equal weighting. It is therefore tempting to link these modes with Sn and Se atomic motions. $\theta_{D2} = 154(2)$ K matches well with the value for Sn obtained from U_{iso} (140(2) K) but $\theta_{D1} = 345(9)$ K is about 75% larger than the value obtained for Se (195(3) K). This suggests that the θ_{Di} might be linked to different structural fragment and this is discussed below. The n_i -weighted inverse cubic average of the obtained θ_{Di} is 186(3) K, which is almost identical to $\theta_D = 189(2)$ K obtained from the low-temperature C_p data using $C_p/T = \gamma + \beta T^2$ [$\beta = 12\pi^4/(5\theta_D^3)$],³³ providing further validation of our model. The origin of the low-temperature Schottky contribution needs further investigation that is outside the scope of this manuscript. There is no evidence for a low-energy Einstein contribution from the data. The absence of such a mode is in keeping with the crystal structure, in which all Sn and Se atoms are connected by at least three strong covalent bonds. The availability of detailed structural and heat capacity data affords an estimate of the acoustic mode Gruneisen parameter using $\gamma = 3\alpha BV/C_v$.³⁴ Here, V is the molar volume C_v is the constant volume heat capacity and the other terms have been defined above. The bulk modulus of SnSe is smaller than e.g. 45 and 40 GPa

for PbSe and PbTe,³⁵ but $\alpha(T)$ is significantly larger. This yields $\gamma = 2.5$ at 300 K, which is in good agreement with calculated values between 2-4 depending on the crystal direction.⁷

Modelling of low-temperature heat capacity data provides important new insight into the link between structure and lattice dynamics. A model using two Debye oscillators of equal abundance was found to give the best fit to the data. This demonstrates that there are two important vibrational energy scales, corresponding to conceptual hard and soft substructures with an equal weighting. As discussed above, $\theta_{D1} = 345(9)$ K and $\theta_{D2} = 154(2)$ K do not directly map onto the values obtained for Sn^{2+} and Se^{2-} from $U_{\text{iso}}(T)$. This suggests that different structural fragments are responsible for the different vibrational energy scales observed here. The Pbnm low-temperature structure has three strong and three weak bonds with bond distances of ~ 2.8 Å and ~ 3.4 Å at 300 K. The Debye temperature (highest phonon frequency) $\theta_D \propto \sqrt{nk/m}$, where n is the number density, k is the bond strength and m is the reduced mass of the oscillator.³³ From the C_p fitting, the number densities of both oscillators are equal and assuming a similar reduced mass, the ratio of the fitted θ_{Di} values is proportional to the square root of the bond strengths. We can approximate the bond strength using bond valence sums,³⁶ which are directly calculated from the Sn-Se bond distances. The BVS ratio is ~ 5 , while the ratio of $\theta_{D1}/\theta_{D2} \approx \sqrt{5}$, signalling an almost perfect agreement between bond strength and the θ_{Di} values. The data therefore suggest that the harder substructure ($\theta_{D1} = 345(9)$ K) is linked to the short bonds, while the softer substructure ($\theta_{D2} = 154(2)$ K) is linked to the weaker bonds within and between the rocksalt layers (Fig 1a). This is a striking result given that lattice vibrations in solids are collective modes involving many atoms and are not individual vibrating bonds.

Computational and inelastic neutron scattering phonon studies show two discrete regions in the phonon density of states (PDOS).⁸⁻¹⁰ A lower band spanning 0-13 meV containing 3 acoustic and 9 optic modes and a higher energy band from 13-25 meV with the remaining 12 optic modes. The upper energies for these two bands correspond very closely to highest phonon frequency for the fitted Debye modes ($k_B\theta_{D1} = 29.7(8)$ meV and $k_B\theta_{D2} = 13.2(2)$ meV). The equal number of phonon

modes in the two bands in the PDOS are in agreement with the equal weighting of the Debye oscillators. It therefore is reasonable to conclude that two Debye modes correspond to the two bands in the PDOS. The phonon calculations reveal that the modes in the lower band are more strongly associated by Sn displacements, with a pronounced peak associated with motions perpendicular to the rocksalt layers.⁹ The higher energy band in the PDOS is more strongly associated with Se displacements. This is consistent with our link to the weak and strong bonds in the crystal structure, where the weaker bonds allow for anharmonic Sn²⁺ displacements.

Heat capacity measurements have been used to reveal that there are two characteristic vibrational energy scales in SnSe corresponding to hard and soft substructures. These distinct substructures arise because of the strong bond divergence in SnSe. Comparison to phonon calculations reveals that the soft substructure is largely responsible for the thermal transport, which is consistent with the strong Umklapp scattering and low thermal conductivities observed for SnSe. This simple link between structure and thermal properties may help with predicting new thermoelectric and thermal barrier materials. Exploring structures with widely diverging bond distances should be a fruitful route to discovering low thermal conductivity materials.

ACKNOWLEDGEMENTS

SRP and JWGB acknowledge the EPSRC (EP/N01717X/1), Leverhulme Trust (RPG-2012-576) and the STFC for provision of beam time at ISIS.

REFERENCES

1. D. M. Rowe, (CRC Press Boca Raton, 2012).
2. K. Biswas, J. Q. He, I. D. Blum, C. I. Wu, T. P. Hogan, D. N. Seidman, V. P. Dravid and M. G. Kanatzidis, *Nature* **489**, 414-418 (2012).
3. G. J. Tan, F. Y. Shi, S. Q. Hao, L. D. Zhao, H. Chi, X. M. Zhang, C. Uher, C. Wolverton, V. P. Dravid and M. G. Kanatzidis, *Nature Communications* **7**, 12167 (2016).
4. H. J. Wu, L. D. Zhao, F. S. Zheng, D. Wu, Y. L. Pei, X. Tong, M. G. Kanatzidis and J. Q. He, *Nature Communications* **5**, 4515 (2014).
5. M. D. Nielsen, V. Ozolins and J. P. Heremans, *Energy & Environmental Science* **6**, 570-578 (2013).

6. S. Lee, K. Esfarjani, T. F. Luo, J. W. Zhou, Z. T. Tian and G. Chen, *Nature Communications* **5**, 3525 (2014).
7. L. D. Zhao, S. H. Lo, Y. S. Zhang, H. Sun, G. J. Tan, C. Uher, C. Wolverton, V. P. Dravid and M. G. Kanatzidis, *Nature* **508**, 373 (2014).
8. C. W. Li, J. Hong, A. F. May, D. Bansal, S. Chi, T. Hong, G. Ehlers and O. Delaire, *Nature Physics* **11**, 1063 (2015).
9. D. Bansal, J. W. Hong, C. W. Li, A. F. May, W. Porter, M. Y. Hu, D. L. Abernathy and O. Delaire, *Physical Review B* **94**, 054307 (2016).
10. R. Q. Guo, X. J. Wang, Y. D. Kuang and B. L. Huang, *Physical Review B* **92**, 115202 (2015).
11. J. M. Skelton, L. A. Burton, S. C. Parker, A. Walsh, C.-E. Kim, A. Soon, J. Buckeridge, A. A. Sokol, C. R. A. Catlow, A. Togo and I. Tanaka, *Physical Review Letters* **117**, 075502 (2016).
12. J. Carrete, N. Mingo and S. Curtarolo, *Applied Physics Letters* **105**, 101907 (2014).
13. H. G. Vonschnering and H. Wiedemeier, *Zeitschrift Fur Kristallographie* **156**, 143-150 (1981).
14. T. Chattopadhyay, J. Pannetier and H. G. Vonschnering, *Journal of Physics and Chemistry of Solids* **47**, 879-885 (1986).
15. P.-C. Wei, S. Bhattacharya, J. He, S. Neeleshwar, R. Podila, Y. Y. Chen and A. M. Rao, *Nature* **539**, E1-E2 (2016).
16. L.-D. Zhao, S.-H. Lo, Y. Zhang, H. Sun, G. Tan, C. Uher, C. Wolverton, V. P. Dravid and M. G. Kanatzidis, *Nature* **539**, E2-E3 (2016).
17. D. Ibrahim, J.-B. Vaney, S. Sassi, C. Candolfi, V. Ohorodniichuk, P. Levinsky, C. Semprimoschnig, A. Dauscher and B. Lenoir, *Applied Physics Letters* **110**, 032103 (2017).
18. C. L. Chen, H. Wang, Y. Y. Chen, T. Day and G. J. Snyder, *Journal of Materials Chemistry A* **2**, 11171-11176 (2014).
19. S. Sassi, C. Candolfi, J. B. Vaney, V. Ohorodniichuk, P. Masschelein, A. Dauscher and B. Lenoir, *Applied Physics Letters* **104**, 212105 (2014).
20. T.-R. Wei, G. Tan, X. Zhang, C.-F. Wu, J.-F. Li, V. P. Dravid, G. J. Snyder and M. G. Kanatzidis, *Journal of the American Chemical Society* **138**, 8875-8882 (2016).
21. L. D. Zhao, C. Chang, G. J. Tan and M. G. Kanatzidis, *Energy & Environmental Science* **9**, 3044-3060 (2016).
22. Q. Zhang, E. K. Chere, J. Sun, F. Cao, K. Dahal, S. Chen, G. Chen and Z. Ren, *Advanced Energy Materials* **5**, 1500360 (2015).
23. S. R. Popuri, M. Pollet, R. Decourt, F. D. Morrison, N. S. Bennett and J. W. G. Bos, *Journal of Materials Chemistry C* **4**, 1685-1691 (2016).
24. Y. X. Chen, Z. H. Ge, M. J. Yin, D. Feng, X. Q. Huang, W. Y. Zhao and J. Q. He, *Advanced Functional Materials* **26**, 6836-6845 (2016).
25. K. L. Peng, X. Lu, H. Zhan, S. Hui, X. D. Tang, G. W. Wang, J. Y. Dai, C. Uher, G. Y. Wang and X. Y. Zhou, *Energy & Environmental Science* **9**, 454-460 (2016).
26. L. D. Zhao, G. J. Tan, S. Q. Hao, J. Q. He, Y. L. Pei, H. Chi, H. Wang, S. K. Gong, H. B. Xu, V. P. Dravid, C. Uher, G. J. Snyder, C. Wolverton and M. G. Kanatzidis, *Science* **351**, 141-144 (2016).
27. S. R. Popuri, A. D. Fortes, I. Loa and J. W. G. Bos, in-preparation (2017).
28. S. Kastbjerg, N. Bindzus, M. Sondergaard, S. Johnsen, N. Lock, M. Christensen, M. Takata, M. A. Spackman and B. B. Iversen, *Advanced Functional Materials* **23**, 5477-5483 (2013).
29. A. Benti, E. Nishibori, S. Paschen and B. B. Iversen, *Physical Review B* **71**, 144107 (2005).
30. O. Delaire, A. F. May, M. A. McGuire, W. D. Porter, M. S. Lucas, M. B. Stone, D. L. Abernathy, V. A. Ravi, S. A. Firdosy and G. J. Snyder, *Physical Review B* **80**, 184302 (2009).

31. I. Loa, R. J. Husband, R. A. Downie, S. R. Popuri and J. W. G. Bos, *Journal of Physics-Condensed Matter* **27**, 072202 (2015).
32. S. A. Hayward, S. A. T. Redfern and E. K. H. Salje, *Journal of Physics-Condensed Matter* **14**, 10131-10144 (2002).
33. N. W. Ashcroft and N. Mermin, D, *Solid State Physics*. (Thomson Learning, 1976).
34. D. T. Morelli, V. Jovovic and J. P. Heremans, *Physical Review Letters* **101**, 035901 (2008).
35. J. M. Skelton, S. C. Parker, A. Togo, I. Tanaka and A. Walsh, *Physical Review B* **89**, 205203 (2014).
36. I. D. Brown and D. Altermatt, *Acta Crystallographica Section B-Structural Science* **41**, 244-247 (1985).